Inorg. Chem. **2003**, *42*, 6404–6411

Inorganic Chemistry
Article

Sonochemical Fabrication and Characterization of Stibnite Nanorods

Hui Wang,[†] Yi-Nong Lu,[‡] Jun-Jie Zhu,*,[†] and Hong-Yuan Chen[†]

Laboratory of Mesoscopic Materials Science and State Key Laboratory of Coordination Chemistry, Department of Chemistry, Nanjing University, Nanjing 210093, P. R. China, and College of Materials Science and Engineering, Nanjing University of Technology, Nanjing 210009, P. R. China

Received March 11, 2003

Regular stibnite (Sb_2S_3) nanorods with diameters of 20–40 nm and lengths of 220–350 nm have been successfully synthesized by a sonochemical method under ambient air from an ethanolic solution containing antimony trichloride and thioacetamide. The as-prepared Sb_2S_3 nanorods are characterized by employing techniques including X-ray powder diffraction, X-ray photoelectron spectroscopy, scanning electron microscopy, energy-dispersive X-ray analysis, transmission electron microscopy, selected area electron diffraction, high-resolution transmission electron microscopy, and optical diffuse reflection spectroscopy. Microstructural analysis reveals that the Sb_2S_3 nanorods crystallize in an orthorhombic structure and predominantly grow along the (001) crystalline plane. High-intensity ultrasound irradiation plays an important role in the formation of these Sb_2S_3 nanorods. The experimental results show that the sonochemical formation of stibnite nanorods can be divided into four steps in sequence: (1) ultrasound-induced decomposition of the precursor, which leads to the formation of amorphous Sb_2S_3 nanospheres; (2) ultrasound-induced crystallization of these amorphous nanospheres and generation of nanocrystalline irregular short rods; (3) a crystal growth process, giving rise to the formation of regular needle-shaped nanowhiskers; (4) surface corrosion and fragmentation of the nanowhiskers by ultrasound irradiation, resulting in the formation of regular nanorods. The optical properties of the Sb_2S_3 amorphous nanospheres, irregular short nanorods, needle-shaped nanowhiskers, and regular nanorods are investigated by diffuse reflection spectroscopic measurements, and the band gaps are measured to be 2.45, 1.99, 1.85, and 1.94 eV, respectively.

Introduction

One-dimensional (1D) nanostructures, such as nanorods, nanowires, nanoribbons, and nanotubes, are known to have many fascinating physical properties and are of great importance in both basic scientific research and potential technological applications.[1] Many unique and interesting properties have been proposed or demonstrated for nanoscale 1D materials, such as superior mechanic toughness, higher luminescence efficiency, enhancement of thermoelectric figure of merit, and lowered lasing threshold.[2] 1D nanostructures are also ideal systems for investigating the dependence of electrical transport, optical properties and mechanical properties on size and dimensionality.[3] Thus, downscaling a broad range of materials to 1D nanoscopic structures is currently the focus of rapidly increasing interest.

V−VI group binary chalcogenides ($A_2^{V}B_3^{VI}$; A = As, Sb, Bi; B = S, Se, Te) have attracted much attention due to their good photovoltaic properties and high thermoelectric power, which allow potential applications in optical, electronic, and thermoelectric cooling devices.[4] Sb_2S_3 is a highly anisotropic V−VI group semiconductor with a layered structure parallel to growth direction and crystallizes in an orthorhombic phase.[5] It is an important material in view of its photosen-

---

* To whom correspondence should be addressed. E-mail: jjzhu@nju.edu.cn. Fax: +86-25-3317761. Tel: +86-25-3594976.

[†] Nanjing University.

[‡] Nanjing University of Technology.

(1) For recent reviews, see: (a) Hu, J.; Odom, T. W.; Lieber, C. M. *Acc. Chem. Res.* **1999**, *32*, 435. (b) Patzke, G. R.; Krumeich, F.; Nesper, R. *Angew. Chem., Int. Ed.* **2002**, *41*, 2446.

(2) (a) Wong, E. W.; Sheehan, P. E.; Lieber, C. M. *Science* **1997**, *277*, 1971. (b) Duan, X. F.; Huang, Y.; Cui, Y.; Wang, J. F.; Lieber, C. M. *Nature* **2001**, *409*, 66. (c) Zhang, Z.; Sun, X.; Dresselhaus, M. S.; Ying, J. Y.; Heremans, J. *Phys. Rev. B* **2000**, *61*, 4850. (d) Huang, M.; Mao, S.; Feick, H.; Yan, H.; Wu, Y.; Kind, H.; Weber, E.; Russo, R.; Yang, P. *Science* **2001**, *292*, 1897.

(3) Yang, P.; Wu, Y.; Fan, R. *Int. J. Nanosci.* **2002**, *1*, 1 and references therein.

(4) Rajpure, K. Y.; Lokhande, C. D.; Bhosale, C. H. *Mater. Res. Bull.* **1999**, *34*, 1079.

(5) Wyckoff, R. W. G. *Crystal structure*, 2nd ed.; Wiley: New York, 1964.

10.1021/ic0342604 CCC: $25.00

sitivity and thermoelectric properties. It finds special applications in target materials for television cameras, microwave switching, paint and polymer industries, and various optoelectric devices.[6] It has also been regarded as a prospective material for solar energy conversion because of its good photosensitivity.[7] Over the past two decades, a variety of experimental approaches have been established to prepare Sb_2S_3, either in the form of powders or solid thin films. Amorphous and polycrystalline Sb_2S_3 films have been prepared by vacuum evaporation[8] and chemical bath deposition.[6,9] However, most of the as-prepared Sb_2S_3 films are amorphous and need to be annealed at high temperatures to crystallize. The solvothermal process has emerged as a powerful tool for generating crystalline Sb_2S_3 powders and systematizing controlled synthesis of morphologies. It has been reported that Sb_2S_3 powders with different morphologies including irregular platelike particles,[10] nanometer- and submicrometer-sized rods,[11] and bulk polygonal tubular crystals[12] can be prepared under solvothermal conditions. Nanostructural stibnite−amine composites have also been prepared by employing self-assembled organic amine templates.[13]

Currently, the study of physical and chemical effects of ultrasound irradiation is a rapidly growing research area. When liquids are irradiated with high-intensity ultrasound irradiation, acoustic cavitations (the formation, growth, and implosive collapse of the bubbles) provide the primary mechanism for sonochemical effects. During cavitation, bubble collapse produces intense local heating, high pressures, and extremely rapid cooling rates.[14] These transient, localized hot spots can drive many chemical reactions, such as oxidation, reduction, dissolution, decomposition, and promotion of polymerization.[15] Some of the most important recent aspects of sonochemistry have been its applications in the synthesis and modification of both organic and inorganic materials.[16] The acoustic cavitation serves as an effective means for concentrating the diffuse energy of ultrasound into a unique set of extreme conditions to produce novel materials with unusual properties. Ultrasound irradiation offers an attractive method for the preparation of nanodimensional materials and has shown rapid growth in its application to nanomaterials science due to its unique reaction effects. Up to now, various kinds of nanodimesional inorganic materials have been synthesized sonochemically, such as metals,[14,17] carbides,[18] nitrides,[19] oxides,[20] chalcogenides,[21] and core/shell nanocomposites.[22]

In this study, we use high-intensity ultrasound irradiation to induce the preferential 1D growth of Sb_2S_3 along the (001) crystalline plane and have successfully prepared Sb_2S_3 nanorods. The as-prepared Sb_2S_3 nanorods are characterized by X-ray powder diffraction (XPRD), X-ray photoelectron spectroscopy (XPS), scanning electron microscopy (SEM), energy-dispersive X-ray analysis (EDAX), transmission electron microscopy (TEM), selected area electron diffraction (SAED), high-resolution transmission electron microscopy (HRTEM), and optical diffuse reflection spectroscopy (DRS). The procedure of the sonochemical formation of the Sb_2S_3 nanorods has also been investigated.

Experimental Section

All the reagents used in our experiments were of analytical purity and were used without further purification. Anhydrous antimony trichloride ($SbCl_3$) was purchased from Beijing Chemical Reagents Factory (Beijing, China). Thioacetamide (CH_3CSNH_2) was purchased from Nanjing chemical reagents factory (Nanjing, China). Absolute ethanol and acetone were purchased from Shanghai chemical reagents factory (Shanghai, China).

In a typical procedure, 0.45 g of anhydrous antimony trichloride and 0.50 g of thioacetamide were dissolved in 50 mL of absolute ethanol in an 100 mL two-necked round-bottom flask. Then the mixture solution was exposed to high-intensity ultrasound irradiation under ambient air for 120 min. Ultrasound irradiation was accomplished with a high-intensity ultrasonic probe (Xinzhi Co., Xinzhi, China; 1.2 cm-diameter; Ti-horn, 20 kHz, 100 W/cm^2)

---

(6) Mane, R. S.; Lokhande, C. D. *Mater. Chem. Phys.* **2000**, *65*, 1.

(7) Nair, M. T. S.; Nair, K.; Garcia, V. M.; Pena, Y.; Arenas, O. L.; Garcia, J. C.; Gomez-Daza, O. *Proc. SPIE-Int. Soc. Opt. Eng.* **1997**, *3138*, 186.

(8) (a) Ghosh, C.; Varma, B. P. *Thin Solid Films* **1979**, *60*, 61. (b) Mahanty, S.; Merino, J. M.; Leon, M. *J. Vac. Sci. Technol., A* **1997**, *15*, 3060.

(9) (a) Lokhande, C. D. *Indian J. Pure Appl. Phys.* **1991**, *29*, 300. (b) Desai, J. D.; Lokhande, C. D. *J. Non-Cryst. Solids* **1995**, *181*, 70. (c) Desai, J. D.; Lokhande, C. D. *Bull. Electrochem. Sci.* **1993**, *9*, 242. (d) Desai, J. D.; Lokhande, C. D. *Thin Solid Films* **1994**, *237*, 29. (e) Mane, R. S.; Sankapal, B. R.; Lokhande, C. D. *Thin Solid Films* **1999**, *353*, 29. (f) Savadogo, O.; Mandal, K. C. *J. Electrochem. Soc.* **1992**, *139* (*1*), L16. (g) Savadogo, O.; Mandal, K. C. *Sol. Energy Mater. Sol. Cells* **1992**, *26*, 117. (h) Nair, M. T. S.; Pena, Y.; Campos, J.; Garcia, V. M.; Nair, P. K. *J. Electrochem. Soc.* **1998**, *145*, 2113.

(10) Yu, S. H.; Shu, L.; Wu, Y. S.; Qian, Y. T.; Xie, Y.; Yang, L. *Mater. Res. Bull.* **1998**, *33*, 1207.

(11) Yang, J.; Zeng, J. H.; Yu, S. H.; Yang, L.; Zhang, Y. H.; Qian, Y. T. *Chem. Mater.* **2000**, *12*, 2924.

(12) Zheng, X.; Xie, Y.; Zhu, L.; Jiang, X.; Jia, Y.; Song, W.; Sun, Y. *Inorg. Chem.* **2002**, *41*, 455.

(13) Neeraj; Rao, C. N. R. *J. Mater. Chem.* **1998**, *8*, 279.

(14) Suslick, K. S.; Choe, S. B.; Cichowlas, A. A.; Grinstaff, M. W. *Nature* **1991**, *353*, 414.

(15) Suslick, K. S. *Ultrasound: Its Chemical, Physical and Biological Effects*; VCH: Weinhein, Germany, 1988.

(16) Suslick, K. S.; Price, G. J. *Annu. Rev. Mater. Sci.* **1999**, *29*, 295 and the references therein.

(17) For examples, see: (a) Koltypin, Y.; Katabi, G.; prozorov, R.; Gedanken, A. *J. Non-Cryst. Solids* **1996**, *201*, 159. (b) Nagata, Y.; Mizukoshi, Y.; Okitsu, K.; Maeda, Y. *Radiat. Res.* **1996**, *146*, 333. (c) Okitsu, K.; Mizukoshi, Y.; Bandow, H.; Maeda, Y.; Yamamoto, T.; Nagata, Y. *Ultrason. Sonochem.* **1996**, *3*, S249.

(18) For examples, see: (a) Hyeon, T.; Fang, M.; Suslick, K. S. *J. Am. Chem. Soc.* **1996**, *118*, 5492. (b) Suslick, K. S.; Hyeon, T.; Fang, M. *Chem. Mater.* **1996**, *8*, 2172.

(19) Koltypin, Y.; Cao, X.; Prozorov, R.; Balogh, J.; Kaptas, D.; Gedanken, A. *J. Mater. Chem.* **1997**, *7*, 2453.

(20) For examples, see: (a) Cao, X.; Koltypin, Yu.; Katabi, G.; Felner, I.; Gedanken, A. *J. Mater. Res.* **1997**, *12*, 402. (b) Dhas, N. A.; Gedanken, A. *J. Phys. Chem. B* **1997**, *101*, 9495. (c) Kumar, R. V.; Diamant, Y.; Gedanken, A. *Chem. Mater.* **2000**, *12*, 2301. (d) Patra, A.; Sominska, E.; Ramesh, S.; Koltypin, Yu.; Zhong, Z.; Minti, H.; Reisfeld, R.; Gedanken, A. *J. Phys. Chem. B* **1999**, *103*, 3361.

(21) For examples, see: (a) Mdleleni, M. M.; Hyeon, T.; Suslick, K. S. *J. Am. Chem. Soc.* **1998**, *120*, 6189. (b) Sostaric, J. Z.; Caruso-Hobson, R. A.; Mulvaney, P.; Grieser, F. *J. Chem. Soc., Faraday Trans.* **1997**, *93*, 1791. (c) Zhu, J. J.; Koltypin, Y.; Gedanken, A. *Chem. Mater.* **2000**, *12*, 73. (d) Wang, H.; Zhu, J. J.; Zhu, J. M.; Chen, H. Y. *J. Phys. Chem. B* **2002**, *106*, 3848. (e) Harpenness, R.; Palchik, O.; Gedanken, A.; Palchik, V.; Amiel, S.; Slifkin, M. A.; Weiss, A. M. *Chem. Mater.* **2002**, *14*, 2094.

(22) For examples, see: (a) Dhas, N. A.; Zaban, A.; Gedanken, A. *Chem. Mater.* **1999**, *11*, 806. (b) Dhas, N. A.; Gedanken, A. *Appl. Phys. Lett.* **1998**, *72*, 2514. (c) Breen, M. L.; Dinsmore, A. D.; Pink, R. H.; Qadri, S. B.; Ratna, B. R. *Langmuir* **2001**, *17*, 903.

immersed directly in the reaction solution. During the reaction, one of the two necks of the flask was linked to the ultrasonic probe and sealed, and the other one was connected with a condensation tube. The sonication was conducted without cooling so that the temperature of the reactant mixture increased gradually during the sonication and a temperature of 333 K was reached at the end of the reaction. When the reaction was finished, a dark brown precipitate was obtained. After cooling of the sample to room temperature, the precipitate was separated by centrifuging at a rotation rate of 10000 rounds/s, washed with absolute ethanol, distilled water, and acetone in sequence, and dried in air at room temperature. The final product was in the form of dark brown powders and was characterized by XPRD, XPS, SEM, EDAX, TEM, SAED, HRTEM, and DRS.

X-ray powder diffraction (XPRD) measurements were performed on a Shimadzu XD-3A X-ray diffractometer with graphite-monochromatized Cu Kα radiation ($\lambda = 0.154\ 18$ nm) and nickel filter. The acceleration voltage was 35 kV with a 150 mA current flux. Scatter and diffraction slits of 0.5 mm and collection slits of 0.3 mm were used. XRD were taken of the powders attached to a glass slide, and data were collected in the 2θ range from 20 to 65°, with a scanning rate of 4°/min and a sample interval of 0.02°. X-ray photoelectron spectra (XPS) were recorded on an ESCALAB MK II X-ray photoelectron spectrometer, using nonmonochromatized Mg Kα X-ray as the excitation source and choosing C 1s (284.6 eV) as the reference line. Scanning electron micrograph (SEM) and energy-dispersive X-ray analysis (EDAX) patterns were taken on a JSM-6301F scanning electron microscopy, operated at 30 kV. Transmission electron micrograph (TEM) and selected area electron diffraction (SAED) patterns were recorded on a JEOL-JEM 200CX transmission electron microscope, using an accelerating voltage of 200 kV. High-resolution transmission electron micrographs (HRTEM) were obtained by employing a JEOL-2010 high-resolution transmission electron microscope with a 200 kV accelerating voltage. A conventional CCD video camera was employed to digitize the micrographs, which was then processed using Digital Micrograph software. The point-to-point resolution was 0.19 nm, and lattice resolution was 0.144 nm. The samples used for TEM and HRTEM observations were prepared by dispersing some products in ethanol followed by ultrasonic vibration for 15 min and then placing a drop of the dispersion onto a copper grid coated with a layer of amorphous carbon. Diffuse reflection spectra (DRS) were recorded on a Shimadzu UV-2100 recording spectrophotometer scanning from 850 to 350 nm at room temperature. The scanning rate was 500 nm/min, and $BaSO_4$ was used as a reference.

Results and Discussion

Characterizations of the Stibnite Nanorods. XPRD measurements were carried out to determine the crystalline phase of the as-prepared powders. The XPRD pattern of the product is shown in Figure 1. All the diffraction peaks can be indexed to be a pure orthorhombic phase for Sb_2S_3 with cell parameters of $a = 11.181$, $b = 11.289$, and $c = 3.830$ Å, which are in good agreement with the literature values.[23] The intensities and positions of the peaks match those data reported in the literature very well. No peaks of any other phases are detected, indicating the high purity of the product.

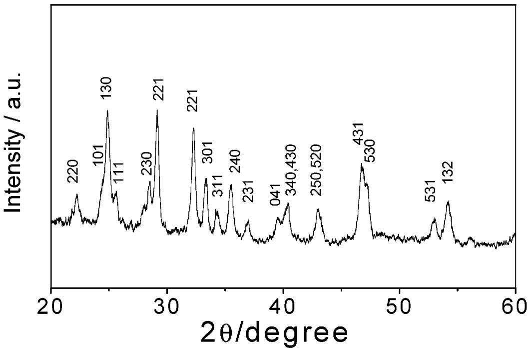

Figure 1. XPRD pattern of the as-prepared Sb_2S_3 nanorods.

XPS measurements provide further information for the evaluation of the composition and purity of the product. The wide-scan XPS spectrum of the product is shown in Figure 2a. The C 1s binding energy obtained in the XPS analysis is located at 292.7 eV and should be standardized by using C 1s as the reference at 284.6 eV. All other peaks should be calibrated accordingly. No obvious impurities could be detected, indicating that the level of impurities is lower than the resolution limit of XPS. The high-resolution XPS spectra taken for Sb 4d and S 2p regions are shown in Figure 2b,c, respectively. Since the position of Sb 3d binding energy is superposed with that of O 2p binding energy, Sb 4d is taken for characterization. The strong peak located at 41.6 eV is assigned to the Sb 4d binding energy, and the peak measured in the S energy region detected at 169.6 eV is attributed to the S 2p transition, which coincides with the literature data.[24] Peak areas of Sb 4d and S 2p are measured, and quantification of the peaks gives the ratio of the Sb:S atomic ratio to be approximately 1:1.46, which is consistent with the given formula for Sb_2S_3 within the experimental errors.

The dimension and morphology of the product were examined by SEM and TEM measurements. A typical SEM image, shown in Figure 3, reveals that the product presents a rodlike morphology with nanometer-sized diameters. The result of selected area EDAX measurements confirms that the sample area shown in Figure 3 contains only antimony and sulfur atoms, and the atomic ratio of Sb:S is calculated to be 1:1.42, which is in good accordance with the XPS results. A representative TEM image of the as-prepared Sb_2S_3 nanorods (Figure 4a) reveals that this sample is composed of nanorods with diameters of 20−40 nm and lengths of 220−350 nm. The SAED pattern (Figure 4b) recorded on an individual Sb_2S_3 nanorod with a convergent electron beam indicates that the stibnite nanorods exhibit a single-crystalline structure with a preferred growth oriented along the (001) crystalline plane.

HRTEM images recorded on individual nanorods provide further insight into their structures. The HRTEM image of a single Sb_2S_3 nanorod (Figure 5a) exhibits good crystalline and clear lattice fringes. It shows that this Sb_2S_3 nanorod crystallizes in a single-crystalline orthorhombic structure. In addition, we have observed that this Sb_2S_3 nanorod has a very thin fuzzy shell. This is probably due to the amorphous species absorbed on the surface of the crystalline nanorods.

---

[23] *Joint Committee on Powder Diffraction Standards (JCPDS)*; No 6-0474.

[24] Wagner, C. D.; Riggs, W. M.; Davis, L. E.; Moulder J. F.; Muilenberg, B. E. *Handbook of X-ray Photoelectron Spectroscopy*; Perkin-Elmer, Physical Electronics Division: Eden Prairie, Mn, 1979.

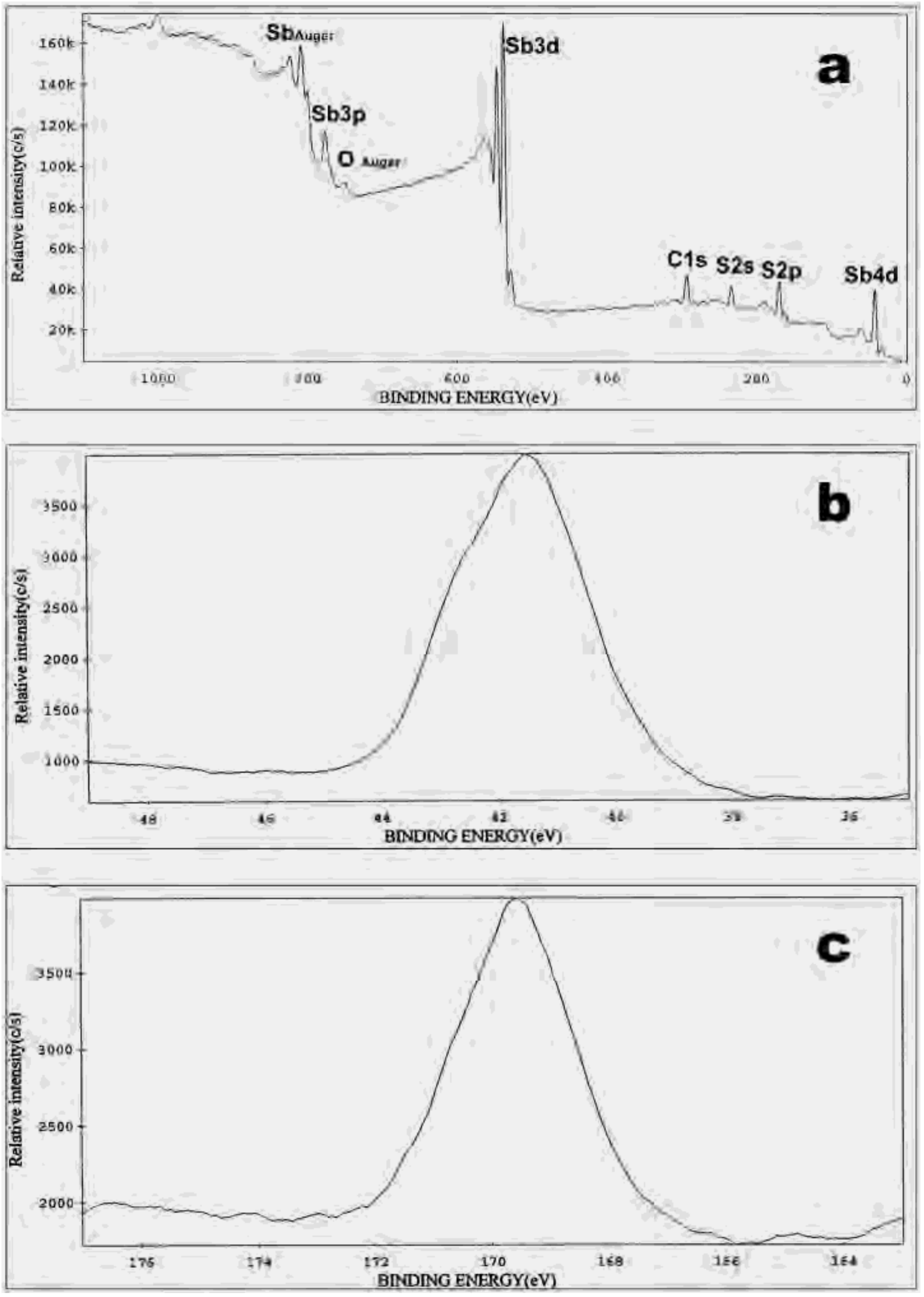

Figure 2. XPS spectra of the as-prepared Sb_2S_3 nanorods: (a) wide scan spectrum; (b) high-resolution spectrum for Sb 4d; (c) high-resolution spectrum for S 2p.

Similarly, a fuzzy shell on the surface of electrochemically deposited CdS nanowires have also been reported previously.[25] In a HRTEM image taken for another Sb_2S_3 nanorod with a higher magnification (Figure 5b), the interplanar spacing is measured to be about 0.38 nm, which corresponds to the (001) plane of the orthorhombic system of Sb_2S_3. The continuous (001) lattice fringes are vertical to the rod axis. On the basis of the HRTEM observations, we are able to draw the conclusion that these Sb_2S_3 nanorods preferentially grow along the (001) direction. The illustration of the structure of the Sb_2S_3 nanorods can be schematically shown in Figure 6.

The study of the optical properties of the materials provides a convenient and effective method for explaining some important features concerning the band structures. The importance of crystal dimensions in the quantum dot size regime is expressed in the variation of the semiconductor energy level structure. To investigate these properties, optical transmission or reflection spectra are most commonly measured. Since our product is in the form of powders, we employed diffuse reflection spectroscopy measurements as the characterization tool. We have measured the optical DRS of the as-prepared Sb_2S_3 nanorods to resolve the excitonic or interband (valence-conduction band) transitions of this sample, which allows us to calculate the band gap. The diffuse reflection spectrum of the Sb_2S_3 nanorods measured

---

(25) Xu, D.; Xu, Y.; Chen, D.; Guo, G.; Gui, L.; Tang, Y. *Chem. Phys. Lett.* **2000**, *325*, 340.

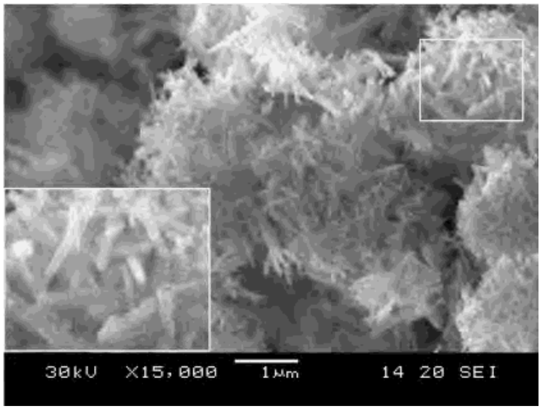

Figure 3. Typical SEM image of the as-prepared Sb_2S_3 nanorods.

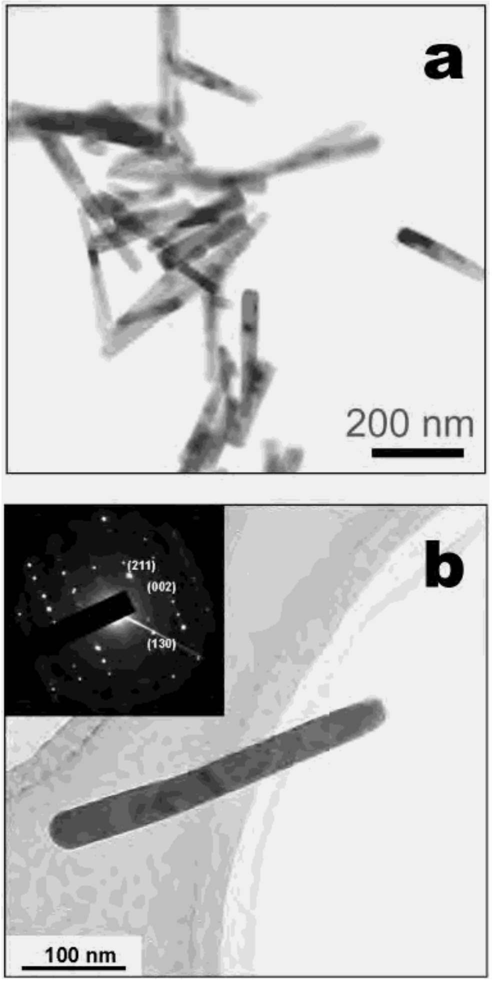

Figure 4. (a) Typical TEM image of the as-prepared Sb_2S_3 nanorods. (b) TEM image of an individual Sb_2S_3 nanorod. The inset is the SAED pattern recorded on this rod.

at room temperature is shown in Figure 7a. The curve ascends sharply from the wavelength at about 800 nm, and the optical absorption edge is approximately located at 650 nm. An estimation of the band gap value is obtained by the intersection point of the tangent of the absorption edge with the extended line of the diffuse reflection at lower wavelength. The as-obtained band gap value is 1.94 eV, which is larger than the reported data of 1.75 eV for Sb_2S_3 bulk material.[9g] Figure 7b shows the diffuse reflection spectrum

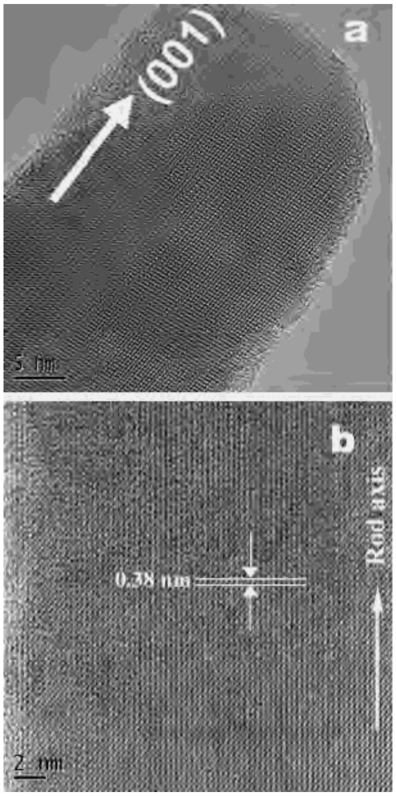

Figure 5. (a) HRTEM image of an individual Sb_2S_3 nanorod. (b) HRTEM image with a higher magnification, revealing the microstructure inside an Sb_2S_3 nanorod.

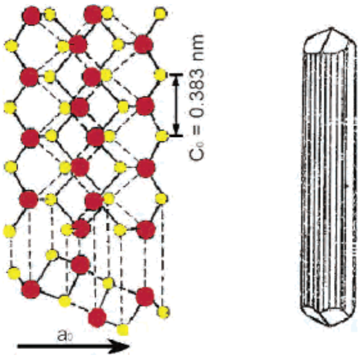

Figure 6. Schematic illustration of the structure of an Sb_2S_3 nanorod. The red spheres represent the S atoms, and the yellow spheres represent the Sb atoms. It is viewed along the (010) direction. The nanorod grows along the (001) crystal face.

of another Sb_2S_3 powder sample. This sample was composed of rodlike single crystals with an average diameter of ca. 1.5 μm and length of 20 μm. The band gap of this sample is estimated to be 1.76 eV according to its diffuse reflection spectrum, which is very close to the reported value of Sb_2S_3 bulk materials. Therefore, this sample can be referred to as the Sb_2S_3 bulk crystals. (The preparation procedure and a typical SEM image of these Sb_2S_3 bulk crystals are shown in the Supporting Information.) The increase in the band gap value is an indicative of the quantum size effects that the as-prepared Sb_2S_3 nanorods exhibit. It is known that light absorption leads to an electron in the conduction band and a positive hole in the valence band. In the case of materials with extremely small sizes, they are confined to potential

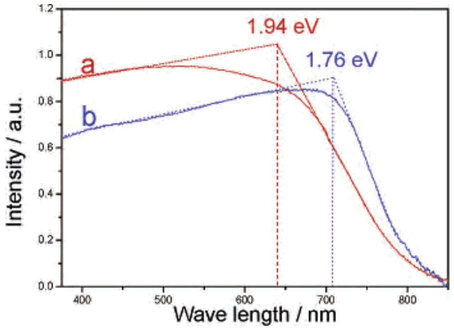

Figure 7. Diffuse reflection spectra of (a) the as-prepared Sb_2S_3 nanorods and (b) rodlike Sb_2S_3 bulk crystals (with average diameter of 1.5 μm and length of 20 μm).

wells of small lateral dimension and the energy difference between the position of conduction band and a free electron, which leads to a quantilization of their energy levels. This phenomenon arises when the dimensions of the materials become comparable to the Broglie wavelength of a charge carrier. During the past decade, the band gaps of Sb_2S_3 solid thin films have received much investigation. Sb_2S_3 thin films with band gaps ranging from 1.62 to 1.87 eV have been prepared and well characterized by a variety of research groups.[9] However, reports on the band gaps of Sb_2S_3 powders are relatively scarce. To the best of our knowledge, only band gaps of tubular Sb_2S_3 crystals (10−15 mm in length, 50−60 μm in width, 5−10 μm in thickness, band gap energy = 1.72 eV)[12] and solvothermally prepared Sb_2S_3 rods (average diameter of ~100 nm and length of ~5 μm, band gap energy = 1.75 eV)[11] have been reported. In the present case, since the sonochemically synthesized Sb_2S_3 nanorods have much smaller diameters, the band gap is larger than those reported.

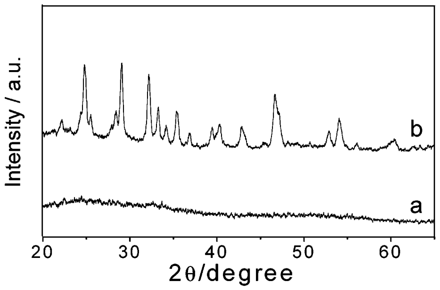

Figure 8. XPRD patterns of the Sb_2S_3 powders obtained after sonication for (a) 30 min and (b) 60 min.

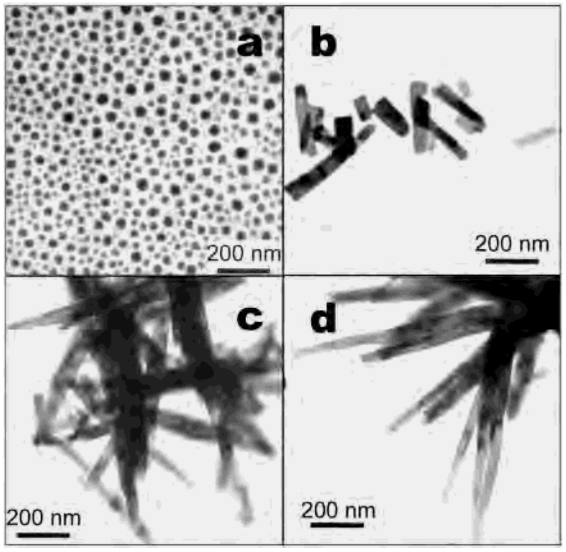

Figure 9. TEM images of the Sb_2S_3 powders obtained after sonication for (a) 30 min, (b) 60 min, (c) 75 min, and (d) 90 min.

Sonochemical Formation of Stibnite Nanorods. Thermal degradation of metal complexes with sulfur-containing ligands seems to be an attractive method for the synthesis of metal sulfides. Several reports refer to thiolato, dithiocarbamate, and thiourea complexes.[26,27] However, such routes require the use of H_2S or H_2/H_2S at high temperatures. It has been known that antimony salts can react with some organic compounds containing a C═S bond, such as thiourea, thioacetamide, ethylxanthate, and tris(*N*,*N*′-disubtituted dithiocabmate), to produce complexes which has the tendency to decompose at suitable temperature or pressure to produce Sb_2S_3 powders.[11] In this study, it was found that when antimony trichloride and thioacetamide were introduced into absolute ethanol, a yellow complex was formed, which we employed as the precursor for the sonochemical formation of the stibnite nanorods. To investigate the details about the sonochemical conversion from the precursor to the final stibnite nanorods, we have carried out a series of experiments by employing different sonication time without changing other preparation conditions. It was found that the original reactant mixture turned into red slurry after about 20 min of sonication. After sonication for 30 min, a red precipitate was collected. EDAX measurement reveals that this red precipitate was pure Sb_2S_3. No diffraction peak was detected in the XPRD pattern of this sample (Figure 8a), indicating that the Sb_2S_3 powders obtained after 30 min sonication was amorphous. A typical TEM image (Figure 9a) reveals that the amorphous Sb_2S_3 is composed of monodisperse nanospheres with diameters in the range of 25−40 nm. During the sonication, bubble collapse in liquid results in an enormous concentration of energy from the conversion of kinetic energy of the liquid motion into heating of the contents of the bubbles. The high local temperatures and pressures provide favorable conditions for driving the decomposition of the antimony−thioacetamide complex, giving rise to the formation of Sb_2S_3. It has been known that there are two regions of sonochemical activity, as postulated by Suslick and co-workers.[28] One is the inside of the collapsing bubbles, where elevated temperatures (several thousands of degrees) and high pressures (hundreds of atmospheres) are produced; the other is the interfacial region

---

(26) (a) Osakada, K.; Yamamoto, T. *Inorg. Chem.* **1991**, *30*, 2328. (b) Osakada, K.; Yamamoto, T. *J. Chem. Soc., Chem. Commun.* **1987**, 1117. (c) Shaw, R. A.; Woods, W. K. *J. Chem. Soc. A* **1971**, 1569.

(27) Wold, A.; Dwight, K. *J. Solid Sate Chem.* **1992**, *96*, 53. (b) Abboudi, M.; Mosset, A. *J. Solid Stae Chem.* **1994**, *109*, 70. (c) Cui, H.; Pike, R. D.; Kershaw, R.; Dwight, K.; Wold. A. *J. Solid State Chem.* **1992**, *101*, 115.

(28) (a) McNamara, W. B., III; Didenko, Y. T.; Suslick, K. S. *Nature* **1999**, *401*, 772. (b) Suslick, K. S.; Hammerton, D. A.; Cline, R. E. *J. Am. Chem. Soc.* **1986**, *108*, 5641. (c) Grinstaff, M. W.; Cichowlas, A. A.; Choe, S. B.; Suslick, K. S. *Ultrasonics* **1992**, *30*, 168.

Table 1. Sb_2S_3 Powders Obtained after Sonication for Different Times

sonication time, s	crystalline phase	morphology	mean dimens, nm	band gap, eV
30	amorphous	monodisperse nanospheres	30	2.45
60	orthorhombic phase	irregular short nanorods		1.99
90	orthorhombic phase	needle-shaped nanowhiskers	35 × 500	1.85
120	orthorhombic phase	regular nanorods	30 × 250	1.94

between the cavitation bubbles and the surrounding bulk solution. Though the temperature in the interfacial region is much lower than the interior of the collapsing bubbles, it is still high enough to rupture chemical bonds and induce a variety of reactions. If the reaction takes place inside the collapsing bubbles, the product obtained is amorphous as a result of the extremely rapid cooling rate ($>10^{10}$ K/s) which occurs during the collapse. On the other hand, if the reaction takes place within the interfacial region, one would expect to get nanocrystalline products.[28,29] In the present case, since amorphous Sb_2S_3 powders were obtained, we propose that the formation of Sb_2S_3 probably occurs inside the collapsing bubbles.

We have also carried out experiments by prolonging the sonication time (Table 1). It was observed that the color of the slurry changed gradually from red into dark brown after 45 min of sonication, indicating the formation of crystalline Sb_2S_3 powders.[30] This was proven by the results of the XPRD measurements. As obviously indicated in Figure 8b, the Sb_2S_3 powders obtained after 60 min of sonication crystallize in a pure orthorhombic structure. It is noteworthy that the amorphous Sb_2S_3 nanospheres converted into irregular short nanorods after sonication for 60 min. The dimensions of these irregular nanorods increased gradually with the prolongation of sonication time, as can be obviously seen in the TEM images (Figure 9b–d). After sonication for 90 min, regular needle-shaped nanowhiskers with diameters of 30–45 nm and lengths over 500 nm could be obtained. High-intensity ultrasound irradiation was found to play a critical role in the crystallization of the amorphous Sb_2S_3 and the preferential 1D growth of the Sb_2S_3 nanocrystals. During ultrasound irradiation of liquid–powder slurries, cavitations and shock waves it creates can accelerate solid particles to high velocities.[31] The interparticle collisions that result are capable of inducing striking changes in morphology, composition, and reactivity of the solids. During the interparticle collisions, the particles can be driven together at sufficiently high speeds to induce effective melting at the point of collision. The energy generated during collision can induce the crystallization of the amorphous Sb_2S_3 particles. In the process of crystallization, Sb_2S_3 presents a preferential 1D growth along the (001) crystal face. It was reported that temperature, pressure, and reaction time played important roles in the solvothermal fabrication of submicron- or nanoscale-sized Sb_2S_3 rods.[11] Only when the reaction was carried out in sealed systems at temperatures of above 393 K where high pressures were available and only when the reaction time was over 6 h could Sb_2S_3 rods be formed. Otherwise only irregular particles could be obtained. In this study, we applied ultrasound irradiation to induce the 1D growth of the Sb_2S_3 nanocrystals and it was found that Sb_2S_3 nanowhiskers could be successfully prepared in an open system. The transient high-temperature and high-pressure field produced during ultrasound irradiation provide a favorable environment for the 1D growth of the Sb_2S_3 nanocrystals, though the bulk solution surrounding the collapsing bubbles is at ambient temperature and atmospheric pressure. To make a comparison, we have also carried out the reaction with vigorous electromagnetic stirring at room temperature instead of ultrasound irradiation. As a result, no Sb_2S_3 could be obtained even after 5 h of reaction. We also failed to get Sb_2S_3 nanowhiskers if the reaction mixture was refluxed under atmospheric pressure even for over 5 h. Instead, only amorphous Sb_2S_3 powders could be obtained. The unusual chain-type structure of Sb_2S_3[32] also played a critical role in the formation of the nanowiskers. Once amorphous Sb_2S_3 began to crystallize, the in-situ-generated Sb_2S_3 nuclei would connect with each other and self-assemble to form chain-type structures. High temperature and high pressure produced by acoustic cavitation is favorable for the self-assembly of these nuclei, leading to the 1D preferential growth of the Sb_2S_3 nanocrystals.

It was found that an interesting phenomenon arose when the sonication time was prolonged to over 2 h. The TEM image (Figure 4a) reveals that the dimensions of the Sb_2S_3 whiskers decreased conspicuously when the sonication time was prolonged to 120 min, and the needle-shaped nanowhiskers were converted into regular and uniform nanorods. The decrease in dimensions may be related to the surface corrosion and fragmentation of solids in the presence of high-intensity ultrasound irradiation. The physical effects of ultrasound cavitations in liquid–solid systems are primarily responsible for the enhancement of the generation of surface damage at the liquid–solid interface by shock waves or microjets and fragmentation of friable solids to increase the surface area. The impingement of microjets or shock waves on the solid surface creates the localized erosion, which is responsible for the ultrasound cleaning and many other sonochemical effects on heterogeneous reactions. The importance of this process to corrosion phenomenon of metals and machinery has already been thoroughly reviewed.[33] Meanwhile, for brittle materials, especially layered inorganic sulfides and oxides, interparticle collisions can also induce fragmentation.[16] This can substantially increase the available surface area of the powders and thus enhance the liquid–

---

(29) Jeevanandam, P.; Koltypin, Y.; Gedanken, A.; Mastai, Y. *J. Mater. Chem.* **2000**, *10*, 511.

(30) In *Handbook of Chemical Reagents*, 2nd ed.; Shanghai Science and Technology Press: Shanghai, China, 1985; p 122.

(31) Doktycz, S. J.; Suslick, K. S. *Science* **1990**, *247*, 1067.

(32) Wells, A. F. In *Inorganic Structure Chemistry*; Wiley: New York, 1977; Chapter 20, p 907.

(33) Preece, C. M.; Hansson, I. L. *Adv. Mech. Phys. Surf.* **1981**, *1*, 199.

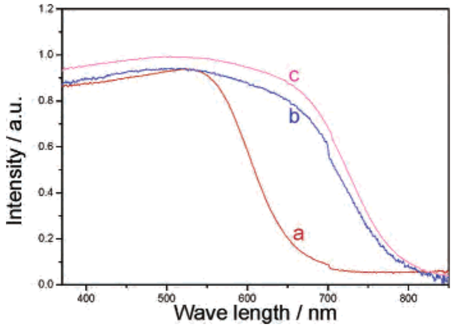

Figure 10. Diffuse reflection spectra of the Sb_2S_3 powders obtained after sonication for (a) 30 min, (b) 60 min, and (c) 90 min.

solid reactions. As mentioned above, since the interparticle collisions are both responsible for the crystal growth and the corrosion/fragmentation of the crystalline solids, the growth and corrosion/fragmentation of the Sb_2S_3 nanocrystals coexisted and competed with each other during sonication in such a liquid−solid heterogeneous system. To make further investigations, the sonication time was even prolonged to 180 and 240 min. However, it was found that the size and morphology of Sb_2S_3 nanorods kept almost unchanged. Therefore, we may draw the conclusion that an equilibrium between the growth and corrosion/fragmentation of the Sb_2S_3 nanorods has been established after sonication for 120 min and the as-prepared stibnite nanorods have become stable in such a sonochemical environment.

Figure 10 shows the diffuse reflection spectra of the stibnite powders obtained after sonchemical reaction for different periods of time. The band gaps of the Sb_2S_3 powders obtained after sonication for 30, 60, and 90 min were calculated to be 2.45, 1.99, and 1.85 eV, respectively. It is noteworthy that when the amorphous Sb_2S_3 was converted into crystalline powders, the absorption edge conspicuously red-shifted and the band gap decreased significantly. It is interesting to note that the band gap of this material decreases with the amorphous−crystalline transition of the powders. A similar decrease in band gaps has been observed previously in the same material and some other chalcogenides.[8,9] Mahanty et al.[8b] and Yang et al.[11] reported that this could be attributed to the higher degree of crystallinity and the increase in the grain size due to the amorphous−crystalline transition. The band gap of the Sb_2S_3 obtained after 60 min of sonication is larger than that of the product obtained after 90 min, which is in accordance with the rule that the band gap of nanosized semiconductors decreases with the increase of dimensions. We have also noticed that the band gap value of the Sb_2S_3 nanowhiskers (90 min product) is smaller than that of the nanorods obtained after 120 min. This can be attributed to the decrease in dimensions of the Sb_2S_3 nanocrystals due to the surface corrosion and fragmentation caused by ultrasound irradiation.

Conclusions

In summary, a novel sonochemical method for the fabrication of Sb_2S_3 nanorods has been successfully established by sonicating an ethanolic solution containing antimony trichloride and thioacetamide under ambient air. The composition, morphology, dimensions, microstructures, and optical properties are characterized. The details about procedure of the sonochemical formation of the Sb_2S_3 nanorods are also investigated. Carrying out experiments with different sonication times allows Sb_2S_3 with different crystallinity, dimensions, and morphologies, including amorphous nanospheres, crystalline irregular short rods, regular needle-shaped nanowhiskers, and regular nanorods, to be obtained. This sonochemical method provides a new route to fabricate Sb_2S_3 nanorods which is fast, convenient, and efficient. It is also promising to be extended to the fabrication of some other nanoscale 1D functional inorganic materials.

Acknowledgment. This work is supported by the National Natural Science Foundation of China (Grant Nos. 50072006 and 90206037), the Jiangsu Advanced Science and Technology Program of PR China (BG 2001039), the Doctoral Foundation of Ministry of Education of China (20020284022), and "863" Project (No. 2003AA302740). The authors thank Mr. Jianmin Hong and Ms. Xiaoshu Wang from the Modern Analytic Center at Nanjing University for their help in TEM and XPS measurements. Kind assistance offered by Mr. Shu Xu, Ms. Wenbo Zhao, and Mr. Yu Zhao from the Department of Chemistry at Nanjing University is also gratefully acknowledged.

Supporting Information Available: The selected area EDAX pattern of the Sb_2S_3 nanorods depicted in Figure 3, a typical SEM image, and the preparation procedure of the rodlike Sb_2S_3 bulk crystals whose diffuse reflection spectrum is shown in Figure 7b. This material is available free of charge via the Internet at http://pubs.acs.org.

IC0342604